ARTICLE

Fabrication of Ni Nanoclusters-Modified Brookite TiO_2 Quasi Nanocubes and Its Photocatalytic Hydrogen Evolution Performance

Peng Zeng[a,c†], Jin-yan Liu[b†], Jin-ming Wang[b], Tian-you Peng[b*]

a. Key Laboratory of Jiangxi University for Applied Chemistry and Chemical Biology, Yichun University, Yichun 336000, China
b. College of Chemistry and Molecular Sciences, Wuhan University, Wuhan 430072, China
c. School of Food and Pharmaceutical Engineering, Zhaoqing University, Zhaoqing 526061, China

(Dated: Received on December 22, 2018; Accepted on February 28, 2019)

The development of low-cost, earth-abundant and highly-efficient cocatalysts is still important to promote the photocatalytic H_2 evolution reaction over semiconductors. Herein, a series of Ni nanoclusters (NCs) modified brookite TiO_2 quasi nanocubes (BTN) (marked as Ni/BTN) are fabricated via a chemical reduction process. It is found that the loading content and oxidation state of Ni NCs can significantly influence the optical absorption, photocatalytic activity, and stability of Ni/BTN composites. Among the resultant Ni NCs-loaded products, 0.1%Ni/BTN composite delivers the best H_2 evolution activity (156 μmol/h), which is 4.3 times higher than that of the BTN alone (36 μmol/h). Furthermore, the Ni NCs with ultrafine size (∼2 nm) and high dispersity enable shorter charge transfer distance by quickly capturing the photoexcited electrons of BTN, and thus result in the improved activity even though the oxidization of some Ni NCs on BTN is harmful to the activity for H_2 evolution due to the much lower electron capturing capability of NiO than metallic Ni. This study not only clarifies that brookite TiO_2 would be a promising high-efficient photocatalyst for H_2 evolution, but also reveals vital clues for further improving its photocatalytic performance using low-cost Ni-based cocatalyst.

Key words: Brookite titania, Nickel nanocluster, Hydrogen evolution reaction, Cocatalyst, Photocatalyst

I. INTRODUCTION

Photocatalytic hydrogen (H_2) evolution process over semiconductors has been considered as a potential technique to address the current energy shortage and environmental problems [1−6]. In recent decades, TiO_2-based photocatalysts have been intensively explored because of its excellent properties such as low cost, good physicochemical stability, and easy availability [2−5]. Among the naturally existing TiO_2 polymorphs (anatase and brookite), thermodynamically metastable brookite is rarely studied because of the preparation difficulty of its pure phase [7, 8]. Nevertheless, the larger bandgap energy and more negative conduction band level than anatase and rutile suggest that brookite should have better photoactivity [9, 10]. Therefore, many efforts have been made to attain pure brookite TiO_2 with various morphologies for exploring its photocatalytic application [11−17].

In 2012, brookite TiO_2 nanoplates with high phase purity were synthesized by varying the hydrothermal reaction condition, which exhibited better photodegradation activity of methyl orange than anatase and rutile under the same surface area [11]. Also, brookite nanosheets exposed four {210}, two {101} and two {201} facets, displaying excellent activity of organic contaminant photodegradation [12]. Moreover, it was reported that brookite nanorods with a lower surface area showed higher H_2 evolution activity than anatase nanoparticles [13]. Similarly, pure brookite nanorods showed better activity for CO_2 reduction than the commercial brookite TiO_2 powder, and the photoactivity depends on the aspect ratio of nanorods [14], respectively. These previous researches demonstrated that brookite TiO_2 would have potential application in the field of photocatalysis, but its activity is still limited by the rapid charge recombination just like the extensively used anatase TiO_2 [13−17].

One of the most popular approaches to overcoming the obstacle of charge recombination is to load cocatalyst since it can not only promote the separation of photoexcited charge carriers, but also reduce the surface activation energy and overpotential loss of photocatalytic reactions [2−4]. Although precious metals (such as Pt, Pd, or Au) are excellent cocatalysts for H_2 evolution t-

†These authors contributed equally to this work.
*Author to whom correspondence should be addressed. E-mail: typeng@whu.edu.cn

,hey can also catalyze the backward reaction. Instead, low-cost transition metals are more intriguing cocatalysts since they will not cause the backward reaction [2−4]. Therefore, various non-precious cocatalysts (such as Cu [18−21], Co [22], Ni [22−25] or their compounds [26−28]) have been explored for promoting the H_2 evolution reactions. Among them, metallic Ni as H_2-evolution cocatalyst has attracted much attention due to its advantages such as earth-abundance, cheapness, non-toxicity, and large work function (∼5.35 eV) that is close to the precious metals such as Pt (∼5.65 eV), Pd (∼5.55 eV), and Au (∼5.10 eV) [29]. It means that Schottky junction can also form between Ni and semiconductors to promote the charge separation [30−33]. For instance, 0.5 wt% Ni nanoclusters with size of 1−2 nm loaded on TiO_2 nanoparticles (P25) caused a H_2 evolution activity superior to a 2.0 wt% Au-loaded TiO_2 due to the high cocatalyst dispersion in the Ni/TiO_2 system [24]. Similarly, Ni nanoclusters with a diameter of 2−3 nm efficiently promoted the photoexcited electron transfer of graphene oxide (GO), and then obviously improved the visible-light-driven H_2 evolution activity of GO [25]. Also, many other Ni-containing compounds such as NiO [25, 34], NiS/NiS_2 [31, 35−38], Ni_2P [39−42], $Ni(OH)_2$ [28, 43, 44]. and Ni complexes [45], have been demonstrated to be highly efficient and stable cocatalysts for the photocatalytic H_2 evolution reaction.

Also, brookite TiO_2 quasi nanocubes (marked as BTN) were fabricated via a hydrothermal method in our group [16], and the Ag-loading caused the BTN to deliver a significantly improved CO_2 reduction activity [17]. It is similar to the previous report [14], wherein photodeposition of Ag or Au nanoparticles on brookite TiO_2 nanorods resulted in a significant improvement in CH_3OH evolution activity because the deposited metal particles work as reductive sites for the multi-electron CO_2 reduction reaction [14]. Herein, this home-made BTN was used as a photocatalyst since there are few reports on brookite TiO_2-based photocatalysts for H_2 evolution so far [13, 21]. By using a facile chemical reduction process, a series of Ni nanoclusters (NCs) modified BTN (Ni/BTN) were synthesized, and a significantly enhanced photocatalytic performance for H_2 evolution compared to single BTN were gained. Also, the effects of the loading content and oxidation state of Ni NCs on the optical absorption, photocatalytic H_2 evolution activity and stability of Ni/BTN composites were discussed in detail.

II. EXPERIMENTS

A. Material preparation

1. Preparation of brookite TiO_2 quasi nanocubes

According to our previous report [16], brookite TiO_2 quasi nanocubes (BTN) were fabricated via hydrothermal treatment of $TiCl_4$ (15.0 mmol) solution at 200 °C for 20 h, which was obtained by droping $TiCl_4$ (15.0 mmol) solution into an ice-water mixture (40 g) in a Teflon cup under stirring, and then urea (5.0 g) and sodium lactate solution (60%, 5.0 mL) were dropped into the Teflon cup in sequence under stirring. After washing with water and alcohol for several times, the resultant precipitate was dried in vacuum at 70 °C for 12 h, and then calcined at 500 °C for 3 h to obtain the BTN product.

2. Preparation of Ni/BTN composites

By using $NaBH_4$ as a reductive reagent, Ni/BTN composites were synthesized as follows: BTN (0.24 g) was dispersed in water (50 mL) containing $Ni(NO_3)_2$ solution (0.1 mol/L, 0.30 mL), and then $NaBH_4$ (0.10 g) was added into the suspension. After stirring for 3 h, the resultant solid was centrifuged and washed with water and alcohol for several times, and then dried in vacuum at 70 °C overnight to obtain 1.0 mol% Ni-loaded BTN (1.0%Ni/BTN). By varying the addition amount of $Ni(NO_3)_2$ solution, a series of Ni/BTN composites with different Ni-loading contents (0.5 mol%, 1.0 mol%, 2.0 mol%, 5.0 mol%, and 10.0 mol%) were obtained.

For comparison, NiO-modified BTN (NiO/BTN) was prepared by calcining the 1.0%Ni/BTN in air at 200 °C for 2 h. Also, 1.0%$Ni(OH)_2$-modified BTN ($Ni(OH)_2$/BTN) was synthesized by dispersing the BTN powder in a NaOH solution (0.25 mol/L, 50 mL), followed by adding $Ni(NO_3)_2$ solution (0.1 mol/L, 0.30 mL) under stirring for 3 h. After washing with water and alcohol for several times, the resultant solid was dried in vacuum at 70 °C overnight to obtain 1.0%$Ni(OH)_2$/BTN.

B. Material characterization

1. Routine characterizations

The X-ray powder diffraction (XRD) patterns of products were obtained using a Mini-flex 600 X-ray diffractometer with Cu Kα irradiation (λ=0.154 nm) working at 40 kV, 15 mA and a scan rate of 4°/min, and a Bruker S4 Pioneer X-ray fluorescence (XRF) spectrometer with an Rh target without standard sample was used to determine the element components. The morphologies of products were observed using a Zeiss-Sigma field emission scanning electron microscope (FESEM) and a JEOL JEM 2100F high-resolution transmission electron microscope (HRTEM) working at 200 kV. A Thermo Fisher ESCALAB 250Xi X-ray photoelectron spectroscope equipped with a standard and Al Kα monochromatic source was used to record the X-ray photoelectron spectra (XPS). UV-Vis diffuse reflectance absorption spectra (DRS) and photolumines-

DOI:10.1063/1674-0068/cjcp1812287

cence (PL) spectra of products were measured using a Shimadzu UV-3600 UV-Vis-NIR spectrophotometer and a Hitachi F4600 fluorometer, respectively.

The photocurrent-time curves were collected in a 50 mL of photocatalyst (0.025 g) suspension containing NaOH (1.9 g) and methyl viologen (6.0 mg) using a three-electrode system, in which a Pt wire, a saturated Ag/AgCl electrode and a Pt gauze electrode were served as a working, a reference, and a counter electrode, respectively. The suspension was continuously purged by N_2 to remove O_2, and then illuminated using a 300 W Xe-lamp. The working electrode was held at +0.5 V *vs.* Ag/AgCl by using a CHI 618 workstation during the photocurrent-time curve determination.

2. Photocatalytic activity tests

The photoreaction experiments for H_2 evolution were performed in a closed photoreactor (pyrex glass, a total volume of 75 mL). Typically, the photocatalyst was dispersed in a sacrificial reagent solution (10 mL), the pH value was adjusted using dilute HCl solution if necessary. The photoreactor containing the photocatalyst suspension was sonicated for several minutes, and thoroughly degassed to remove air entirely, and then illuminated using a 300 W Xe-lamp (PLS-SXE300, Beijing Trusttech Co. Ltd., China). A gas chromatograph (GC, SP-6800A, TCD, 5 Å molecular sieve columns and Ar carrier) was used to determine the H_2 evolved amount. For the long-term photoreaction experiments, the photocatalyst after the first run of 4 h was recovered for the next run through centrifugation and washing with water for several times, and then dried in vacuum at 70 °C.

III. RESULTS AND DISCUSSION

A. Crystal phase and composition analyses

The XRD patterns of the single brookite TiO_2 quasi nanocubes (BTN) and its Ni-loaded products (Ni/BTN) are displayed in FIG. 1. As seen, all XRD patterns of those products are well-conformed to the orthorhombic brookite TiO_2 (PDF No.29-1360), in which the diffraction peaks at 2θ=25.3°, 25.7°, 30.8°, 36.2°, 37.3°, 40.1°, 42.4°, 46.0°, 48.0°, and 49.1° can be readily due to the (210), (111), (211), (102), (021), (202), (221), (302), (321), and (312) plane's reflections of brookite TiO_2 [16, 17], respectively. There is no diffraction peak that can be ascribable to anatase or rutile, suggesting that the BTN in those Ni-loaded products still remains a high phase purity even through the present post-loading process of Ni species on the pristine BTN.

In addition, no diffraction peak of metallic Ni or its oxides can be detected in the XRD patterns of those

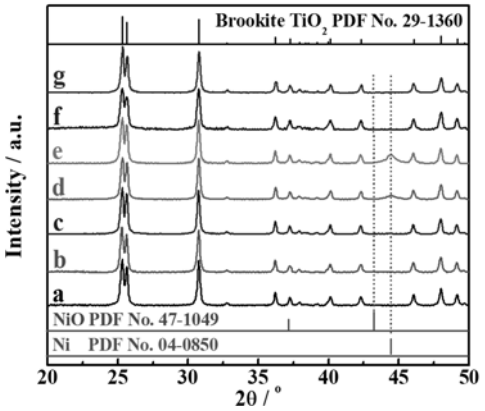

FIG. 1 XRD patterns of (a) the pristine BTN, (b) 0.5%Ni/BTN, (c) 1.0%Ni/BTN, (d) 5.0%Ni/BTN, (e) 10%Ni/BTN, (f) 1.0%NiO/BTN, and (g) 5.0%NiO/BTN.

Ni/BTN composites with Ni-loading amount less than 5.0 mol% (FIG. 1). Once the Ni-loading amount is enhanced to 5.0%, a new diffraction peak at 2θ=44.5° that conforms to the (111) plane reflection of cubic Ni (PDF No.04-0850) can be detected from the XRD patterns of those Ni/BTN composites. The increasing peak intensity of metallic Ni along with the increase of Ni-loading content suggests the gradually increased size of the loaded Ni particles on BTN. Moreover, it can be concluded that no Ni species is doped into the crystal lattice of BTN because all diffraction peaks of those Ni/BTN are located at the same positions as the brookite TiO_2. Especially, those NiO/BTN composites derived from the calcination of Ni/BTN in air at 200 °C for 2 h still show no diffraction peak of NiO, implying the high dispersity of NiO species on BTN.

Although the above XRD patterns of Ni/BTN composites with Ni-loading content less than 5.0 mol% show no obvious diffraction peak of metallic Ni (FIG. 1), the loaded Ni species can be confirmed by the element mappings of 0.5%Ni/BTN composite (FIG. S1 in supplementary materials), from which it can be found that Ni element has even distribution in the FESEM observation region. Moreover, the analysis results of element compositions obtained by using X-ray fluorescence (XRF) technique (Table I) indicate that the Ni molar precentages in those Ni/BTN composites are close to their respective original adding amount. The supplementary increasement in the O molar ratio for those Ni/BTN composites with Ni species higher than 2.0 mol% (Table I) might be due to the oxidization of some metallic Ni species on BTN, which will be further discussed below.

X-ray photoelectron spectra (XPS, FIG. 2) are determined and used to further explore the existing states of the loaded Ni particles on BTN. The survey XPS spectrum (FIG. 2(a)) confirms that Ni, Ti, and O elements exist in 1.0%Ni/BTN composite, and the high resolution Ti2p XPS spectrum (FIG. 2(b)) displays two

DOI:10.1063/1674-0068/cjcp1812287

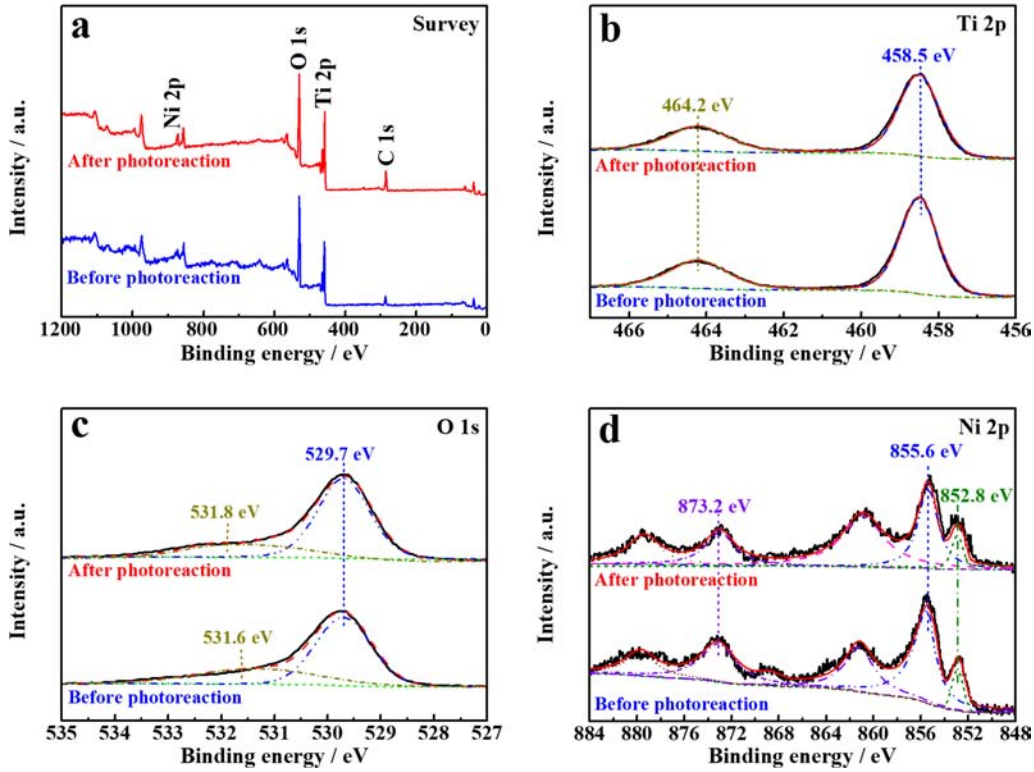

FIG. 2 (a) Survey, (b) Ti2p, (c) O1s, and (d) Ni2p XPS spectra of 1.0%Ni/BTN composite and its recycled product after the 12 h photoreaction.

TABLE I Element compositions of various products detected using XRF spectrometer.

Sample	Element composition/mol%			Ti:O ratio
	Ni	Ti	O	
Pristine BTN		1.25	2.50	1:2.00
1.0%Ni/BTN	0.80	1.24	2.49	1:2.00
2.0%Ni/BTN	1.60	1.22	2.47	1:2.02
5.0%Ni/BTN	4.70	1.19	2.45	1:2.06
10%Ni/BTN	9.70	1.13	2.36	1:2.09

binding energy (BE) peaks at 458.5 eV (Ti $2p_{3/2}$) and 464.2 eV (Ti $2p_{1/2}$) of Ti^{4+} ions in the Ni/BTN composite [17]. The two BE peaks at 529.7 and 531.6 eV deconvolved from the O1s regional XPS spectrum (FIG. 2(c)) of the 1.0%Ni/BTN composite can be due to the lattice oxygen of Ti-O-Ti and surface Ti-OH groups of TiO_2 [17, 46], respectively. The BE peak at 852.8 eV in the Ni 2p regional spectrum (FIG. 2(d)) can be ascribed to metallic Ni species [23, 30], while two BE peaks at 855.6 and 873.2 eV well match with the BE values of Ni $2p_{3/2}$ and Ni $2p_{1/2}$ of Ni^{2+} ions [28, 30], respectively. In addition, those weak BE peaks at ∼861.0 and 880.0 eV on the higher BE sides of Ni $2p_{3/2}$ and Ni $2p_{1/2}$ of Ni^{2+} ions can be due to the characteristic satellite peaks of Ni^{2+} ions [23, 28, 30].

Similarly, it was reported that metallic Cu also coexisted with small amount of CuO in a Cu-modified rutile TiO_2 nanosheets, which was attributed to the oxidization of metallic Cu during the XPS measurement [47]. In the present Ni/BTN composites, however, the BE peak intensities of Ni^{2+} ions are higher than those of Ni^0 (FIG. 2(d)). It implies that the metallic Ni coexists with relatively large amount of NiO species, which are unlikely to be formed during the XPS measurement [28, 30, 48]. Since the redox potential ($E^{\ominus}$=−0.23 V) of Ni^{2+}/Ni is much lower than that ($E^{\ominus}$=+0.34 V) of Cu^{2+}/Cu, it can be concluded that some metallic Ni species on BTN after the chemical reduction process are inevitably oxidized into NiO species during the sample storage and photoactivity measurement, which results in the coexistence of Ni and NiO on BTN to form NiO_x/TiO_2-like products [28, 30].

B. Microstructure analyses

The single BTNs show quasi nanocube-like morphology with round edges, even surfaces and an average diameter of ∼50 nm (FIG. 3(a)). Those BTN particles in the Ni/BTN composites with 1.0 mol%, 5.0 mol%, and 10 mol% Ni-loading amount still maintain their nanocube-like morphology (FIG. 3(b−d)), while some ultrafine nanoparticles can be observed from

DOI:10.1063/1674-0068/cjcp1812287

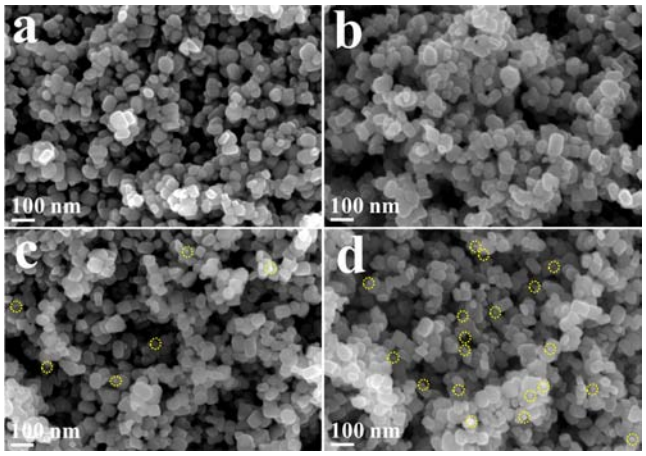

FIG. 3 FESEM images of (a) the pristine BTN, (b) 1.0%Ni/BTN, (c) 5.0%Ni/BTN, and (d) 10%Ni/BTN.

the FESEM image (marked with circles in FIG. 3(c)) of 5.0%Ni/BTN composite, which shows an increasing trend along with further enhancing the Ni-loading content to 10 mol% (FIG. 3(d)). Moreover, the low magnification FESEM images (FIG. S2 in supplementary materials) show that some aggregates appear on BTN surfaces when the Ni-loading content is higher than 5.0 mol%.

TEM image (FIG. 4(a)) also indicates that the single BTN particles have relatively uniform quasi nanocube-like microstructures with even surfaces. Along with the increase of Ni-loading amount, the BTN particle surfaces become coarser (FIG. 4(b−g)), which can be due to the gradually increased amount of Ni species loaded on BTN. HRTEM image (FIG. 4(c)) displays that some Ni nanoclusters (NCs) with ultrafine size of 1−2 nm are tightly modified on the BTN particles in 1.0%Ni/BTN composite. After loading with 5.0 mol% Ni species, more ultrafine NCs can be observed from BTN surfaces (FIG. 4(d)), and the HRTEM image (FIG. 4(e)) indicates that those loaded Ni NCs have slightly increased particle sizes of ∼2 nm. The *d*-spacing of ∼0.204 nm can be measured from the modified ultrafine NCs, and this interplanar distance well-conforms with the (111) crystal lattice of fcc metallic Ni [23, 24]. In addition, a *d*-spacing of 0.352 nm that well-matches to the (210) planes of brookite TiO_2 can also be found from the nanocube-like region [16, 17]. The intimate contact between Ni NCs and BTN can be further observed from the TEM and HRTEM image (FIG. 4(f, g)) of 10%Ni/BTN. Those ultrafine Ni NCs with high surface area and dispersity can shorten the charge transfer distance by quickly capturing the photogenerated electrons of BTN [18], which would be a benefit to the H_2 evolution as discussed below.

Although the TEM and HTEM images (FIG. 4(b−g)) show that those Ni NCs have slightly increased particle sizes and denser distribution on BTN with enhancing the Ni-loading contents, the sizes of those Ni NCs are still smaller than 3.0 nm even for those composites with Ni-loading content higher than 2.0 mol%. Moreover, no obvious lattice fringe of NiO is observed from the HRTEM images (FIG. 4(c, f, g)) even though the above XPS results demonstrate the co-existence of Ni and NiO in the Ni/BTN composites. It implies that NiO species might be very small or exist as an amorphous form (as shown in the red circles of FIG. 4(g)). For making this issue clear, 10%Ni/BTN composite was calcined in Ar atmosphere at 200 °C for 2 h and used for TEM observation. As seen from FIG. 4(h), the particle sizes of those ultrafine NCs increase obviously, and there are a few lattice stripes (FIG. 4(i)) with *d*-spacings of ∼0.209 nm, corresponding to the (200) lattice of cubic NiO [48]. The above results suggest that those ultrafine Ni NCs are unstable and some of them will be easily oxidized to form NiO NCs with very small sizes and low crystallinity.

C. Optical absorption property analyses

UV-Vis diffuse reflectance absorption spectra (DRS) indicate that the single BTN has an absorption edge at ∼379 nm (FIG. 5), which corresponds to a bandgap energy (E_g) of ∼3.27 eV [16, 17]. Although the Ni/BTN composites display an increasing background absorption in the range of 550−800 nm upon enhancing the Ni-loading contents, the absorption edges of Ni/BTN composites are very similar to those of the single BTN. It suggests that Ni species are not doped into the brookite lattice [28], which is consistent with the above XRD result. Nevertheless, trailing phenomena in the range of 380−550 nm can be observed even though no significant difference exists in the absorption edges among those Ni/BTN composites and BTN alone, which is similar to the previously reported $Ni(OH)_2/TiO_2$ composites [28], in which a new absorption peak at ∼450 nm was attributed to the direct interfacial charge transfer (IFCT) transition process (from TiO_2's VB to Ni^{2+} ions). As mentioned above, Ni NCs in Ni/BTN composites are easily oxidized to form NiO, and thus the trailing phenomena in the range of 380−550 nm may also be due to a similar IFCT transition process in the present Ni/BTN composites [28].

To explore the reason of the increasing background absorption in the range of 550−800 nm along with the increase of Ni-loading contents in those Ni/BTN composites, the DRS spectra of 1.0%Ni/BTN and 1.0%NiO/BTN (derived from calcination of 1.0%Ni/BTN in air at 200 °C) are also listed in inset of FIG. 5. As seen, 1.0%NiO/BTN exhibits an obviously enhanced background absorption in the broad range of 380−800 nm compared to 1.0%Ni/BTN. It also confirms that the above additional absorption bands of Ni/BTN composites can be attributed to the co-existing NiO species, and the elevating background absorptions may be due to the gradually enhanced NiO contents in

DOI:10.1063/1674-0068/cjcp1812287

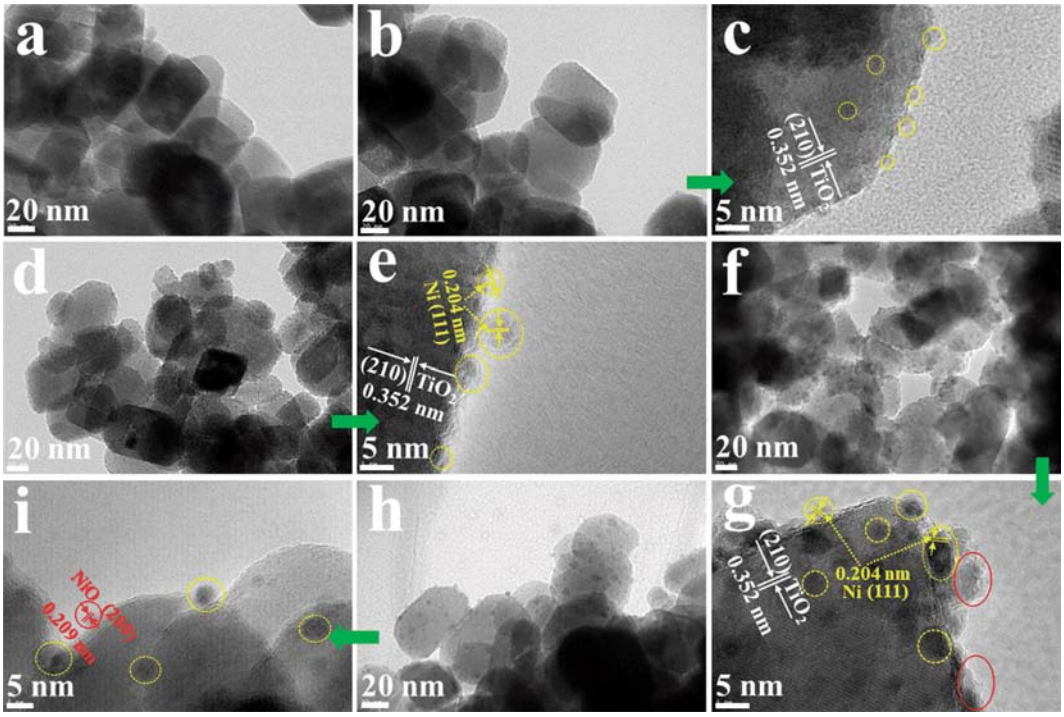

FIG. 4 TEM and HRTEM images of (a) the pristine BTN, (b, c) 1.0%Ni/BTN, (d, e) 5.0%Ni/BTN, (f, g) 10%Ni/BTN and (h, i) 10%Ni/BTN calcined at 200 °C for 2 h under Ar atmosphere.

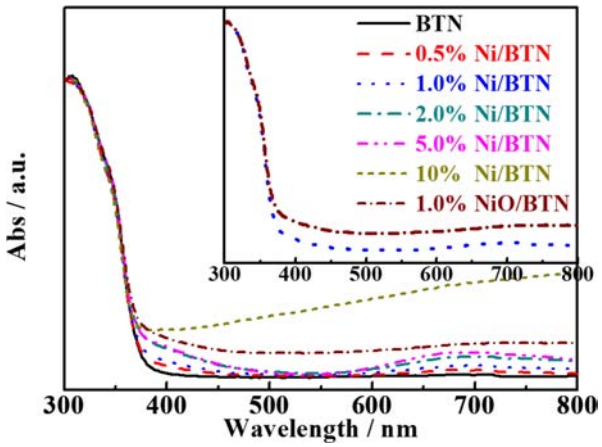

FIG. 5 UV-Vis diffuse reflectance absorption spectra of the pristine BTN and its Ni-loaded products (Ni/BTN) with different Ni-loading contents.

those Ni/BTN composites.

D. Photocatalytic H_2 evolution performance analyses

The optimization of photoreaction conditions of the H_2 evolution system was performed using the 1.0%Ni/BTN composite dispersed in a triethanolamine (TEOA) aqueous solution (10 mL) under Xe-lamp full-spectrum irradiation. The effects of TEOA solution acidity and photocatalyst dosage on the H_2 evolution activity were investigated initially. As seen from FIG. S3(a) in supplementary materials, 1.0%Ni/BTN in the TEOA solution with an initial pH=10.50 only delivers a H_2 evolution activity of 75 μmol/h, which shows an increasing trend upon adjusting the pH value from 10.50 to 6.00 followed by a decreasing one with further enhancing the solution acidity, and thus the maximum H_2 evolution activity (156 μmol/h) was achieved from the 1.0%Ni/BTN dispersed in TEOA solution with pH=6.00. The above changing trends can be due to effects of acidity on the redox potential of H^+/H_2, Fermi level of Ni NCs, surface property (such as surface charge density and adsorption ability) and energy band structures of photocatalyst, and the significant decrease in H_2 evolution activity at pH=2.00 can be attributed to the unstable property of metallic Ni NCs in the strong acidic condition. Also, the photocatalyst dosage influences the H_2 evolution activity of 1.0%Ni/BTN (FIG. S3(b) in supplementary materials), which increases from 111 μmol/h to 156 μmol/h with enhancing the addition amount from 5.0 mg to 10 mg, and then slightly decreases to 135 μmol/h with further enhancing to 15 mg. Therefore, the optimized photoreaction conditions for the present Ni/BTN composites should be 10 mg photocatalyst dispersed in TEOA solution with pH=6.00.

The effect of Ni-loading content on the H_2 evolution activity of Ni/BTN composite under the above optimized photoreaction conditions is depicted in FIG. 6(a).

DOI:10.1063/1674-0068/cjcp1812287

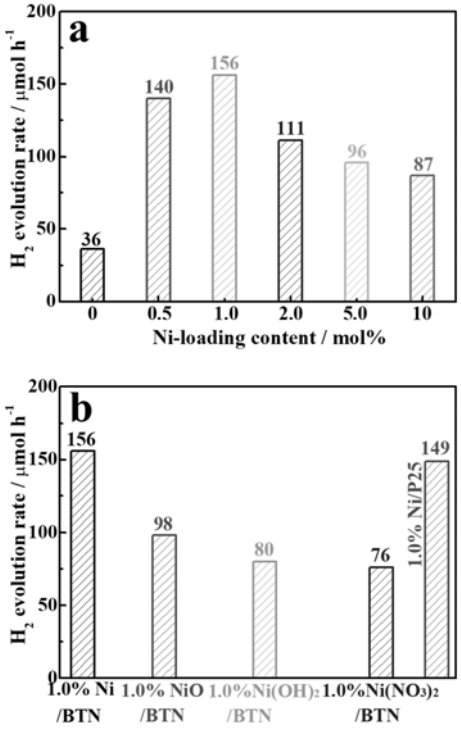

FIG. 6 (a) Photocatalytic H_2 evolution activity of Ni/BTN composites with various Ni-loading contents. (b) Comparison of photocatalytic H_2 evolution activities of various 1.0%Ni-containing cocatalyst-loaded BTN composites and the 1.0%Ni-loaded P25. Conditions: 10 mg catalyst in 10 vol.% TEOA solution (10 mL, pH=6.00) if otherwise stated.

The H_2 evolution activity can be significantly improved from 36 μmol/h (for the single BTN) to 140 μmol/h and 156 μmol/h by loading with 0.5 mol% and 1.0 mol% Ni cocatalyst, respectively. Further enhancing the Ni-loading content, a gradually reduced activity can be observed, and therefore the 1.0%Ni/BTN delivers the maximum H_2 evolution activity (156 μmol/h), which is ca. 4.3 times higher than that (36 μmol/h) of BTN alone. The increasing activity along with the enhancement of the Ni-loading content can be ascribed to the cocatalyst function of those loaded Ni NCs on BTN for promoting the photogenerated charge separation [18], and the overloaded Ni species with larger and denser NCs as shown in FIG. 4 would absorb and/or scatter the incident light, and thus cause that Ni/BTN composite is unable to be excited effectively. The best activity of 1.0%Ni/BTN can be due to the ultrafine Ni NCs with high surface area and dispersity, which can shorten the charge transfer distance by quickly capturing the photoexcited electrons of BTN [18].

To explore the effect of the oxidation states of Ni species on the photoactivity of BTN, 1.0%NiO/BTN, 1.0%$Ni(OH)_2$/BTN and 1.0%$Ni(NO_3)_2$/BTN are also prepared and used as photocatalyst under the same optimial photoreaction conditions. As seen from FIG. 6(b), 1.0%NiO/BTN, 1.0%$Ni(OH)_2$/BTN, and 1.0%$Ni(NO_3)_2$/BTN composites only achieve a H_2 evolution activity of 98, 80, and 76 μmol/h, respectively. All of them are higher than that (36 μmol/h) of BTN alone, but much lower than that (156 μmol/h) of 1.0%Ni/BTN. It indicates that the Ni NCs loaded on BTN have much better cocatalyst function than that of NiO, $Ni(OH)_2$, or even Ni^{2+} ions. Furthermore, the optimal H_2 evolution activity (156 μmol/h) of the 1.0%Ni/BTN composite is slightly higher than that (149 μmol/h) of the 1.0%Ni-loaded commercial TiO_2 nanoparticles (P25, Deggusa) (FIG. 6(b)), which contains mixed crystal of anatase and rutile phases in a ratio of ca. 3:1 with an average particle size of ∼24 nm, and was extensively used as reference in the fields of photocatalysis and dye-sensitized solar cells [49, 50]. This result is consistent with the previous reports on brookite TiO_2 usually exhibiting better photoactivity than anatase or rutile [11−13]. The above results not only demonstrate that brookite TiO_2 should be a promising photocatalyst for efficient H_2 evolution, but also reveal that the low-cost Ni NCs as cocatalysts can efficiently improve the photocatalytic performance of brookite TiO_2.

The photostabilities for the H_2 evolution reaction of 1.0%Ni/BTN and 1.0%NiO/BTN under the optimized photoreaction conditions are investigated in three successive runs, in which each cycle was irradiated for 4 h, and then the photocatalyst was separated, washed and vacuum dried for the nex run. As shown in FIG. 7, the 1.0%Ni/BTN delivers an average H_2 evolution activity of 154, 144, and 136 μmol/h at the 1st, 2nd, and 3rd runs, respectively. As compared to the 1st run, the activity loss of 1.0%Ni/BTN for the 3rd run is estimated to be 11.7%, while the 1.0%NiO/BTN exhibits a much smaller activity loss (4.9%). That is to say, 1.0%Ni/BTN composite displays a much better H_2 evolution activity but slightly lower photostability than 1.0%NiO/BTN due to the easy oxidization feature of Ni NCs as mentioned above. Although some Ni NCs in Ni/BTN composites are inevitably oxidized as demonstrated in the above characterization, the recovered 1.0%Ni/BTN still exhibits a survey XPS spectrum similar to that of the original one without obvious deviation from the locations of the main elements (FIG. 2(a)). Also, the recovered 1.0%Ni/BTN displays the doublet Ti^{4+} peaks of its original one as shown in the Ti 2p XPS spectra (FIG. 2(b)), suggesting the photostablity of BTN [17]. Although there are some differences in the O 1s XPS spectra between the 1.0%Ni/BTN and its recovered product (FIG. 2(c)), the BE values of 531.8 and 529.7 eV ascribed to the hydroxyl adsorbed on the surface and Ti−O−Ti bonds in brookite TiO_2 still can be observed. In addition, the intensity of BE peak ascribed to metallic Ni species at ∼852.8 eV shows a slightly decreasing trend, but the BE peak position of Ni 2p spectrum after the photoreaction has not changed obviously (FIG. 2(d)). Also, the recovered product displays an

DOI:10.1063/1674-0068/cjcp1812287

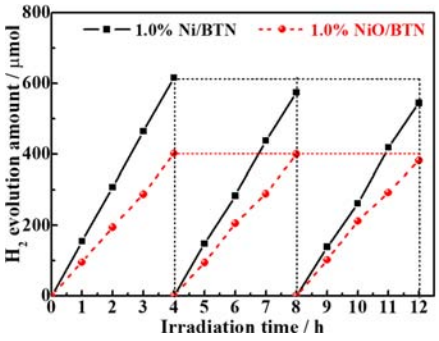

FIG. 7 Typical time course for H_2 evolution over 1.0%Ni/BTN and 1.0%NiO/BTN composites under 300 W Xe-lamp irradiation. Conditions: 10 mg photocatalysts in 10 vol.% TEOA solution (10 mL, pH=6.00).

XRD pattern very similar to the original one (FIG. S4 in supplementary materials). The above results demonstrate that those Ni NCs modified BTN have relatively good stability, and thus would be an inexpensive and highly-efficient photocatalyst for H_2 evolution reaction.

E. General discussion on the photocatalytic mechanism

Since the metallic Ni has a work function of ∼5.35 eV [29], which is much higher than the conduction band (CB) level (∼4.26 eV) of TiO_2 [51], the photoexcited electrons of BTN can transfer to Ni NCs through their intimately contacted interfaces (FIG. 4) from the point of view of thermodynamics, and thus the possible mechanism for H_2 evolution from the Ni/BTN system may be drawn in FIG. 8. The Ni/BTN composite is photoexcited by the incident photons to produce electron-hole pairs, and those loaded Ni NCs can work as electron sinks to capture those photoexcited electrons of BTN to promote the charge separation of the photoreaction system. Those electrons transferred to Ni NCs can further react with protons or water adsorbed on their surface to produce H_2, while the photogenerated holes in BTN lead to the oxidization of those TEOA molecules, and therefore the Ni/BTN composite displays the relatively steady photocatalytic H_2 evolution performance as shown in FIG. 7.

The above proposed charge transfer/separation processes can be confirmed by the photoluminescence (PL) spectra shown in FIG. 9(a). The strong PL peaks (in the range of 350−600 nm) of the single BTN can be due to the fast recombination of photogenerated charge, and the PL quenching effect after modifying with 0.5 mol% Ni NC can be mainly ascribed to the photoexcited electrons transferring from BTN to Ni NCs, which then retards the direct recombination of those photogenerated charge carriers, and thus causes the decreased PL intensity compared to the single BTN. Moreover, the enhanced PL quenching effect along with the increase of Ni-loading content demonstrates that the enhanced

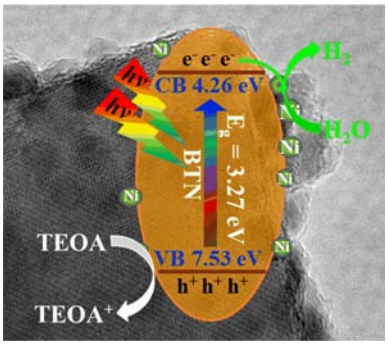

FIG. 8 The possible photocatalytic mechanism for H_2 evolution over the Ni/BTN composite.

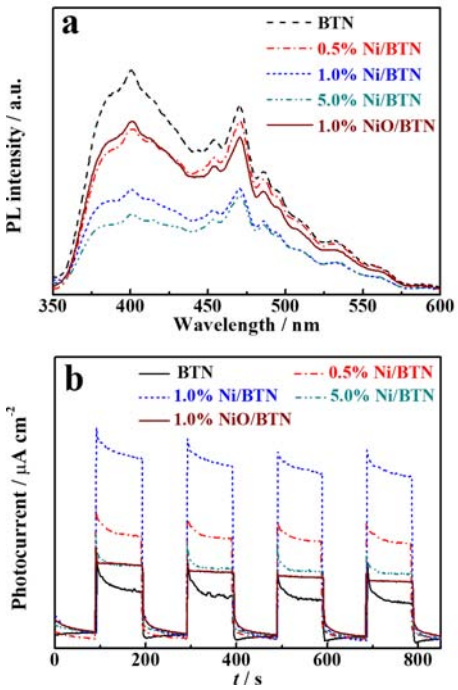

FIG. 9 (a) Photoluminescence spectra of the pristine BTN, NiO/BTN and Ni/BTN composites under excitation wavelength of 290 nm. (b) Photocurrent-time curves of the pristine BTN, NiO/BTN and Ni/BTN composites in NaOH solution under 300 W Xe-lamp irradiation.

Ni-loading contents can further promote the electron transfer, and thus is benefit to the improvement of H_2 evolution activity of Ni/BTN composites as shown in FIG. 6(a). It is worth mentioning that the PL quenching effect of 1.0%NiO/BTN is obviously lower than that of 1.0%Ni/BTN. It infers that the Ni NCs has much strong electron capturing ability compared to NiO NCs [25, 34], which is consistent with the results that the NiO/BTN has much lower photoactivity than Ni/BTN as shown in FIG. 6(b).

Also, the transient photocurrent responses of the single BTN and its Ni-loaded products are recorded to evaluate the charge separation efficiency (FIG. 9(b)).

DOI:10.1063/1674-0068/cjcp1812287

The photocurrent values show an obvious increasing trend with enhancing the Ni-loading contents to 1.0 mol%, and then a decreasing one with further enhancing the Ni-loading content, which is consistent with the changing trends of H_2 evolution activity (FIG. 6(a)). Since the electron capturing ability of metal cocatalysts is generally related to their particle sizes [18], it can be concluded that the Ni NCs in 1.0%Ni/BTN system have more suitable size and surface states to improve the electron capturing efficiency and then the activity of the photoreaction system. Moreover, the photocurrent responses of 1.0%Ni/BTN is much larger than that of NiO/BTN, also indicating that Ni NCs have stronger electron capturing capability than NiO NCs [25, 27].

As mentioned above, the low redox potential ($E^{\ominus}$=−0.23 V) of Ni^{2+}/Ni means that metallic Ni NCs on BTN would be inevitably oxidized into NiO species [28, 30]. It was reported that the photocatalysts loaded with NiO/Ni bilayer structure presented a better H_2 evolution activity than that loaded with Ni or NiO alone [52, 53], which was attributed to the more effective charge separation/transfer in the NiO/Ni double layer structure since NiO has lower Fermi level than metallic Ni. However, our characterization results show that the Ni NCs in Ni/BTN composites have very small particle sizes (∼2 nm) and high dispersity, and thus some Ni NCs are oxidized into NiO with ultrafine size or amorphous form during the sample treatment and storage. Therefore, a similar NiO/Ni bilayer structure was not formed on BTN, and some of Ni NCs are oxidized into NiO as observed from the HRTEM image (FIG. 4). Since NiO has much lower electron capturing capability than metallic Ni [25, 34], the NiO/BTN displays much lower activity than Ni/BTN under the same conditions as shown in FIG. 6(b). Moreover, the oxidization process of some Ni NCs in the present Ni/BTN composites is not conducive to the improvement of photoactivity, and thus it is necessary to seek suitable ways to inhibit this oxidation in the future investigation. Nevertheless, the significantly improved activity of the present Ni NCs-modified BTN demonstrate that brookite TiO_2 would be a promising photocatalyst for efficient H_2 evolution as reported previously [13, 21]. Moreover, the present Ni NCs with ultrafine size and high dispersity should be a potential cocatalyst that can provide low-cost and efficient means of improving the H_2 evolution performance of semiconductors if its oxidation process can be retarded or utilized rationally.

IV. CONCLUSION

In summary, a series of Ni nanoclusters (NCs) modified brookite TiO_2 quasi nanocubes (BTN) composites are fabricated via a chemical reduction process. By varying the loading content and oxidation state of Ni species, the optical absorption, photocatalytic activity, and stability for H_2 evolution can be significantly adjusted. Among them, 0.1%Ni/BTN composite achieves the best H_2 evolution activity (156 μmol/h), which is 4.3 times higher than that (36 μmol/h) of BTN alone. According to the experimental and characterization results, those Ni NCs with ultrafine size (∼2 nm) and high dispersity can offer shorter charge transfer distance by quickly capturing the photoexcited electrons of BTN, and thus cause the significantly improved activity of the Ni NCs-modified BTN. Our work not only confirms that brookite TiO_2 would be a potential photocatalyst for efficient H_2 production, but also provides some vital clues for further improving its photocatalytic performance using low-cost and earth-abundant Ni-based cocatalyst.

Supplementary materials: FESEM image and its element mappings, low magnification FESEM images of pristine BTN and its Ni-loaded products (Ni/BTN), and effects of photoreaction conditions on the activity of 1.0%Ni/BTN composite, and the XRD patterns of 1.0%Ni/BTN composite and its recycled product after 12 h photoreaction are shown in FIG. S1−S4.

V. ACKNOWLEDGMENTS

This work was supported by the National Natural Science Foundation of China (No.21573166 and No.21271146), the Funds for Creative Research Groups of Hubei Province (No.2014CFA007), the Natural Science Foundation of Jiangsu Province (No.BK20151247), the Science Foundation of Jiangxi Provincial Office of Education (No.GJJ180854), and the Post-Doctoral Start-up Project of Yichun University (NACPB20180201), China.

[1] A. Fujishima and K. Honda, Nature **238**, 37 (1972).
[2] J. R. Ran, J. Zhang, J. G. Yu, M. Jaroniec, and S. Z. Qiao, Chem. Soc. Rev. **43**, 7787 (2014).
[3] X. X. Zou and Y. Zhang, Chem. Soc. Rev. **44**, 5148 (2015).
[4] J. H. Yang, D. G. Wang, H. X. Han, and C. Li, Acc. Chem. Res. **46**, 1900 (2013).
[5] X. H. Zhang, T. Y. Peng, and S. S. Song, J. Mater. Chem. A **4**, 2365 (2016).
[6] S. H. Chen, J. J. Wang, J. Huang, and Q. X. Li, Chin. J. Chem. Phys. **30**, 36 (2017).
[7] R. Boppella, P. Basak, and S. V. Manorama, ACS Appl. Mater. Inter. **4**, 1239 (2012).
[8] Y. F. Cao, X. T. Li, Z. F. Bian, A. Fuhr, D. Q. Zhang, and J. Zhu, Appl. Catal. B **180**, 551 (2016).
[9] L. J. Liu, H. L. Zhao, J. M. Andino, and Y. Li, ACS Catal. **2**, 1817 (2012).
[10] M. M. Rodriguez, X. Peng, L. Liu, Y. Li, and J. M. Andino, J. Phys. Chem. C **116**, 19755 (2012).
[11] J. G. Li, T. Ishigaki, and X. D. Sun, J. Phys. Chem. C **111**, 4969 (2007).

DOI:10.1063/1674-0068/cjcp1812287

[12] H. F. Lin, L. P. Li, M. L. Zhao, X. S. Huang, X. M. Chen, G. S. Li, and R. C. Yu, J. Am. Chem. Soc. **134**, 8328 (2012).
[13] T. A. Kandiel, A. Feldhoff, L. Robben, R. Dillert, and D. W. Bahnemann, Chem. Mater. **22**, 2050 (2010).
[14] T. Ohno, T. Higo, N. Murakami, H. Saito, Q. Zhang, Y. Yang, and T. Tsubota, Appl. Catal. B **152/153**, 309 (2014).
[15] L. J. Zhang, V. M. Menendez-Flores, N. Murakama, and T. Ohno, Appl. Surf. Sci. **258**, 5803 (2012).
[16] J. L. Xu, K. Li, S. F. Wu, W. Y. Shi, and T. Y. Peng, J. Mater. Chem. A **3**, 7453 (2015).
[17] K. Li, T. Y. Peng, Z. H. Ying, S. S. Song, and J. Zhang, Appl. Catal. B **180**, 130 (2016).
[18] I. Shown, H. C. Hsu, Y. C. Chang, C. H. Lin, P. K. Roy, A. Ganguly, C. H. Wang, J. K. Chang, C. I. Wu, L. C. Chen, and K. H. Chen, Nano Lett. **14**, 6097 (2014).
[19] W. J. Foo, C. Zhang, and G. W. Ho, Nanoscale **5**, 759 (2013).
[20] S. Obregon, M. J. Munoz-Batista, M. Fernandez-Garcia, A. Kubacka, and G. Colon, Appl. Catal. B **179**, 468 (2015).
[21] J. Y. Liu, J. P. Jin, J. Luo, X. L. Li, L. Zan, and T. Y. Peng, Mater. Today Chem. **1/2**, 23 (2016).
[22] P. D. Tran, J. F. Xi, S. K. Batabyal, L. H. Wong, J. Barber, and J. S. C. Loo, Phys. Chem. Chem. Phys. **14**, 11596 (2012).
[23] W. L. Zhen, J. T. Ma, and G. X. Lu, Appl. Catal. B **190**, 12 (2016).
[24] W. T. Chen, A. Chan, X. D. Sun-Waterhouse, T. Moriga, H. Idriss, and G. I. N. Waterhouse, J. Catal. **326**, 43 (2015).
[25] A. K. Agegnehu, C. J. Pan, J. Rick, J. F. Lee, W. N. Su, and B. J. Hwang, J. Mater. Chem. **22**, 13849 (2012).
[26] S. Cao, Y. Chen, C. C. Hou, X. J. Lv, and W. F. Fu, J. Mater. Chem. A **3**, 6096 (2015).
[27] Y. Xu and R. Xu, Appl. Surf. Sci. **351**, 779 (2015).
[28] J. G. Yu, Y. Hai, and B. Cheng, J. Phys. Chem. C **115**, 4953 (2011).
[29] C. K. Chung, W. T. Chang, and R. X. Zhou, Microsyst. Technol. **14**, 1389 (2008).
[30] L. G. Kong, Y. M. Dong, P. P. Jiang, G. L. Wang, H. Z. Zhang, and N. Zhao, J. Mater. Chem. A **4**, 9998 (2016).
[31] J. Q. Wen, J. Xie, H. D. Zhang, A. P. Zhang, Y. J. Liu, X. B. Chen, and X. Li, ACS Appl. Mater. Inter. **9**, 14031 (2017).
[32] C. Z. Sun, H. Zhang, H. Liu, X. X. Zheng, W. X. Zou, L. Dong, and L. Qi, Appl. Catal. **235**, 66 (2018).
[33] Q. Zhao, J. Sun, S. C. Li, C. P. Huang, W. F. Yao, W. Chen, T. Zeng, Q. Wu, and Q. J. Xu, ACS Catal. **8**, 11863 (2018).
[34] S. I. Fujita, H. Kawamori, D. Honda, H. Yoshida, and M. Arai, Appl. Catal. B **181**, 818 (2016).
[35] W. Zhang, Y. B. Wang, Z. Wang, Z. Y. Zhong, and R. Xu, Chem. Commun. **46**, 7631 (2010).
[36] H. Zhao, H. Z. Zhang, G. W. Cui, Y. M. Dong, G. L. Wang, P. P. Jiang, X. M. Wu, and N. Zhao, Appl. Catal. B **225**, 284 (2018).
[37] X. X. Zhao, J. R. Feng, J. Liu, W. Shi, G. M. Yang, G. C. Wang, and P. Cheng, Angew. Chem. Int. Ed. **57**, 9790 (2018).
[38] F. Chen, H. Yang, X. F. Wang, and H. G. Yu, Chin. J. Catal. **38**, 296 (2017).
[39] A. Indra, A. Acharjya, P. W. Menezes, C. Mershchjann, D. Hollmann, M. Schwarze, M. Aktas, A. Friedrich, S. Lochbrunner, A. Thomas, and M. Driess, Angew. Chem. Int. Ed. **56**, 1653 (2017).
[40] X. L. Li, X. J. Wang, J. Y. Zhu, Y. P. Li, J. Zhao, and F. T. Li, Chem. Eng. J. **353**, 15 (2018).
[41] Z. W. Shao, Y. N. He, T. T. Zeng, Y. N. Yang, X. P. Pu, B. Ge, and J. M. Dou, J. Alloys Compd. **769**, 889 (2018).
[42] Y. B. Chen and Z. X. Qin, Catal. Sci. Technol. **6**, 8212 (2016).
[43] S. Leong, D. Li, K. Hapgood, X. W. Zhang, and H. T. Wang, Appl. Catal. B **198**, 224 (2016).
[44] P. Wang, Y. G. Lu, X. F. Wang, and H. G. Yu, Appl. Surf. Sci. **391**, 259 (2017).
[45] S. W. Cao, Y. P. Yuan, J. Barber, S. C. J. Loo, and C. Xue, Appl. Surf. Sci. **319**, 344 (2014).
[46] B. K. Vijayan, N. M. Dimitrijevic, D. Finkelstein-Shapiro, J. S. Wu, and K. A. Gray, ACS Catal. **2**, 223 (2012).
[47] Y. L. Zou, S. Z. Kang, X. Q. Li, L. X. Qin, and J. Mu, Int. J. Hydrogen Energy **39**, 15403 (2014).
[48] W. Dai, X. H. Pan, S. S. Chen, C. Chen, Z. Wen, H. H. Zhang, and Z. Z. Ye, J. Mater. Chem. C **2**, 4606 (2014).
[49] K. Li, B. Chai, T. Y. Peng, J. Mao, and L. Zan, ACS Catal. **3**, 170 (2013).
[50] J. L. Xu, S. F. Wu, J. H. Ri, J. P. Jin, and T. Y. Peng. J. Power Sources **327**, 77 (2016).
[51] J. G. Yu and J. R. Ran, Energy Environ. Sci. **4**, 1364 (2014).
[52] X. P. Chen, W. Chen, H. Y. Gao, Y. Yang, and W. F. Shangguan, Appl. Catal. B **152/153**, 68 (2014).
[53] M. K. Tian, W. F. Shangguan, J. Yuan, L. Jiang, M. X. Chen, J. W. Shi, Z. Y. Ouyang, and S. J. Wang, Appl. Catal. A **309**, 76 (2006).

DOI:10.1063/1674-0068/cjcp1812287